A Unified Framework for Analysis-Ready Data generation from Resourcesat-2/2A sensors

Keerthi V[1], Suresh Kumar M[1], Radhika T[1], Manju Sarma M[1], Prakash Chauhan[1]

[1]National Remote Sensing Centre, ISRO, Dept. of Space, Hyderabad, India
keerthi_v@nrsc.gov.in, sureshmachikanti@nrsc.gov.in, radhika_t@nrsc.gov.in, manjusarma_s@nrsc.gov.in, director@nrsc.gov.in

Keywords: Atmospheric correction, Radiative transfer code,Top of the atmosphere, Surface reflectance, Analysis Ready Data, RadCalNet

Abstract

More than decadal data is archived by the Indian remote sensing satellite Resourcesat-2 series of sensors. This data holds immense potential for long-term terrestrial monitoring. Harnessing its full potential requires systematic organization of all available observations, necessitating rigorous pre-processing efforts.Analysis Ready Data (ARD) products have streamlined the process of accessing and analyzing satellite imagery, fostering interoperability over time and across various datasets enabling a wide range of applications in environmental monitoring, disaster management, agriculture, urban planning, and scientific research. An optimized frame work is defined for Resourcesat-2/2A images to generate ARD products. The product package contains surface reflectance (SR) and top-of-atmosphere reflectance (TOA) along with pixel quality layer and Metadata file. This paper outlines the procedures undertaken, validation of the techniques and analysis of the obtained results. ARD products are validated for both absolute and relative terms with ground measurements and harmonized Landsat and Sentinel (HLS) data sets and the amount of agreement is around 90% and 95% respectively

1. Introduction

The advent of the Indian remote sensing satellite Resourcesat-2 series has contributed significantly to the archive of terrestrial monitoring data over the past decade. However, to unlock the full potential of this rich dataset, there is a need for systematic organization and rigorous pre-processing. Analysis ready data (ARD) has emerged as a powerful approach to address this issue. The development of ARD products has emerged as a critical step in making satellite imagery more accessiblefor immediate analysis with minimal additional effort. ARD refers to data that has been pre-processed and calibrated to a high degree which is useful for various applications. ARD products ensure interoperability over time and across different datasets, facilitating their use in environmental monitoring, disaster management, agriculture, urban planning, and scientific research (Siqueira A et al., 2019).

There are numerous approaches and frame works for ARD pre-processing (WulderM.A et al., 2019). The Committee on Earth Observation Satellites (CEOS) has established a set of guidelines for ARD processing knows as CARD4L (Lewis A et al., 2018). An ARD framework involves two key processing steps for multiple sensor and time series datasets: radiometric and geometric processing. These two steps are essential for generating accurate and comparable data across multiple images, facilitating more reliable analysis and interpretation of satellite imagery.

Radiometric processing involves calibrating the sensor data by converting the raw digital numbers (DN) to physical units such as radiance or reflectance. Top-of-Atmosphere (TOA) reflectance is an important intermediate product in the processing and serves as a basis for further corrections. TOA is combined effect of surface reflectance and atmospheric influences. Surface reflectance (SR) is a fundamental parameter in remote sensing that pertains to the Earth’s surface in the solar reflective wavelengths (Nazeeret al., 2021). By accounting for atmospheric effects such as scattering and absorption by gases, aerosols, and water vapour, SR enhances the comparability of multiple images over the same region there by aids the detection and characterization of changes in the Earth's surface.

Geometric processing of satellite images involves correcting and transforming the raw images to accurately represent the location on the Earth's surface. This process ensures that the spatial relationships and coordinates in the image are true to real-world geography. Ortho-rectification is the mandatory process to achieve the sub pixel accuracy in building an ARD product.

This paper details the key concepts of ARD processing, generation and validation, highlighting its benefits and outlining the current state-of-the-art techniques.

2. Datasets

Resourcesat-2 (RS2) and its follow-up mission to Resourcesat-2A (R2A) are designed to provide enhanced capabilities to data users using comparable sensors.RS2/R2A features a three-tier imaging capability, boasting a distinctive combination of payloads comprising three solid-state cameras: a high-resolution Linear Imaging Self-Scanning Sensor (L4), alongside two medium-resolution cameras, namely Linear Imaging Self-Scanning Sensor (L3), and an Advanced Wide Field Sensor (AW).RS2 and R2A are launched from India in 2011 and 2016 respectively. Table 1 shows the sensor’s configuration. The L3 sensor encompasses a swath of 140 km, offering a temporal resolution of 24 days and AW sensor spans a swath of 740 km, providing a temporal resolution of 5 days. L4 sensor operates in three spectral bands with a spatial resolution of 5.8m and a swath of 70 km. Temporal resolution is improved to 12 days with seamless combination of both RS2/R2A L3 sensors in the form of ARD. Ortho rectified products generated in near real time are the primary inputs to ARD generation. Synchronous Auxiliary inputs;like Aerosol Optical Depth (AOD), Water

vapour (WV) and Ozone which are required for surface reflectance generation are taken from MODIS sensor. These data sets are downloaded and pre-processed from LAADS DAAC.

3. Methodology

A customized framework is developed to realize ARD generationfrom Resourcesat-2/2A images. The same processing flow is shown in figure 1. CEOS-ARD Guidelines for Surface reflectance Product family specification 5.0.1 are followed to generate final ARD Layers. As per this specification, an ARD is a pack of Surface reflectance, top-of-atmosphere reflectance layers of individual spectral bands, sun-sensor viewing geometry layers along with a self-explainable pixel quality layer and a Metadata file.

The framework involves the following steps:

- TOA Reflectance Calculation: Estimation of reflectance values at the top of the atmosphere using at sensor radiance values
- SR Calculation: Conversion of at sensor reflectance data to surface reflectance values using radiative transfer code.
- Pixel Quality Layer: Generation of a pixel quality layer indicating the reliability of each pixel.
- Metadata File: Creation of a comprehensive meta data file that contains relevant information about the dataset.

Satellite /Sensor	Bands	Wave length (µm)	Spatial Resolution	Temporal Resolution
R2&2A L3/ AWiFS	B2 - Green	0.52 - 0.59	24m /56m	24days/ 5days
	B3 - Red	0.62 - 0.68		
	B4 - NIR	0.77 - 0.86		
	B5 - SWIR	1.55 - 1.70		
R2&2A L4	B2 - Green	0.52 - 0.59	5.8m	5 days
	B3 - Red	0.62 - 0.68		
	B4 - NIR	0.77 - 0.86		

Table1. R2& R2A sensors configuration

3.1 Generation of Top of the Atmosphere

TOA products are generated using (1) pixel level sun-sensor geometry and band convolved exo-atmospheric solar irradiances computed from sensor’s relative spectral response functions (Chavez, 1996).

$$\rho_{TOA} = \frac{L_\lambda \pi d^2}{E_0 \cos\theta} \quad (1)$$

Where
ρ_{TOA}=TOA reflectance
L_λ = at-sensor radiance (mw/sr-cm^2-um)
E_0 =exo-atmospheric sun irradiance value
d = Sun-Earth distance in astronomical units
θ= Zenith Angle

3.2 Generation of Surface Reflectance

Completely automated chain-Atmospheric correction Tool for Resourcesat sensors (ACT-RS) is developed based on Second Simulation of the Satellite Signal in the Solar Spectrum (6S) Radiative Transfer (RT) code which corrects the at-sensor reflectance for scattering and absorbing effects (Vermote et al., 1997). The required inputs for this RT code for accurate estimations of surface reflectance from satellite imagery are at-sensor radiance image, sun-sensor geometry, digital elevation model height, ancillary data-AOD, WV & Ozone. The accuracy of the SR products are depends on the selection of atmospheric and aerosol model. Here, the user-defined (Uw and Uo3) atmospheric model and continental aerosol model was chosen for generation of SR.

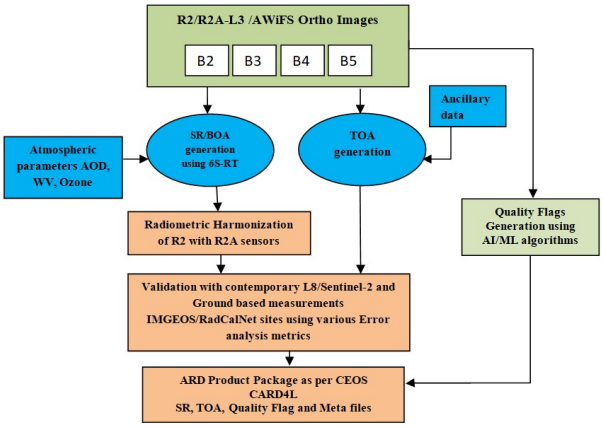

Figure 1. ARD Frame work

3.2.1 Pre-processing of ancillary data: Ancillary data is downloaded from Terra-MODIS atmospheric products (MOD04 and MOD07). Voids in this atmospheric data due to clouds, cloud shadows, snow and homogeneous wide areas result into erroneous surface reflectances and need to be avoided. Mean compositing techniques with various compositing time intervals were adopted to fill these voids. Persistent voids were addressed by preparing climatology data from 20 years of observations and also from Copernicus Atmosphere Monitoring Service (CAMS) Global atmospheric composition forecast products (Garrigues et al.,2022).

3.2.2 Radiometric Harmonization: Radiometric normalization or harmonization ensures consistency between images taken at different times or by different sensors by adjusting for variations in lighting/atmospheric conditions and sensor characteristics. Achieving radiometric harmonization among equivalent sensors of both RS2 and R2A missions is crucial to enable interoperability. Here R2A is used as reference due to its temporal consistency and high degree of closeness to in-situ/ground measurements. The spectral bands and spectral response functions of the RS2 and R2A sensors are almost similar. Therefore, there is no need for spectral pass band adjustment. Several pseudo invariant targets in Indian terrain and CEOS sites covering the entire dynamic range of the sensors over various seasons of five-year period were used for the harmonization. The selection of pseudo invariant targets and radiometric normalization was performed by using IR-MAD algorithm (Cantyet al., 2007). Band wise coefficients are computed and applied to RS2 L3 & AW sensors. L4 sensor is a tiltable camera in across track direction with a maximum amount tilt of ± 26^0. There is a need to correct the Bidirectional Reflectance Distribution Function (BRDF), which accounts for the varying reflectance of surfaces depending on the angle of illumination and observation. After BRDF correction, harmonized coefficients will be computed.

3.3 Generation of Quality layer

Optical images often face challenges due to the presence of clouds and cloud shadows which impede feature extraction. Similarly, hill shadows and zero-fills adversely affect classification accuracy. It's advisable to identify and isolate these corrupted pixels by creating a separate layer. A customized deep Convolution Neural Networks (CNN) architecture, combined with an enhanced U-Net model(Ronneberger et al., 2015)has been tailored and deployed to produce a pixel level quality layer. The training data is manually labelled using threshold-based methods and visual interpretation. This model automatically learns to distinguish features such as water, clouds, cloud shadows, snow, and land. Extensive data sets, featuring images from diverse geographical regions and various seasons are utilized for training and evaluation.

4. Validation

A comprehensive validation of TOA and SR products was carried out to quantify the accuracy. Both absolute and relative validations were conducted by selecting areas with high spatial homogeneity, low atmospheric variability, and a high probability of clear skies. The Error metrics such as root mean square error (RMSE), sum square error (SSE), correlation coefficient (R^2), slope and offsets were computed with respect to the references to assess the accuracy. Ground measurements from India and Radiometric Calibration Network (RCN) are used for absolute validation. Instrumented sites within the RCN provide automated data collections across multiple locations, facilitating inter-comparison among various sensors (Bouvet M et al., 2019). For relative validation, contemporary Surface reflectance products of Harmonized Landsat-Sentinel (HLS) and Sentinel-2A/2B are considered. The spatial resolution of HLS product is 30m; hence products from L3/AW are comparable. Due to high spatial resolution, L4 products are validated with level-2A products of Sentinel-2A/2B.

TOA products are also validated with the computed TOA measurements over RCN, other mentioned ground targets and with Landsat-8/Sentinel-2 TOA products.

Quality layer was validated with visual interpretation. The proposed CNN-Unet model achieved a classification accuracy of 92%. The architecture was initially trained using TOA images from the RS2/R2A AW sensor, and transfer learning techniques were applied to L3/L4 sensor data. A sample quality layer of R2A L3 sensor is depicted infigure 2.

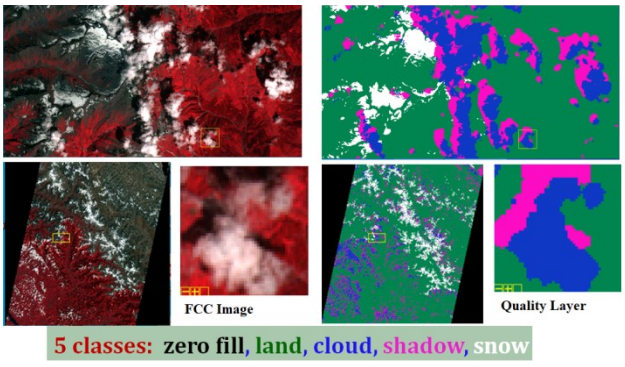

Figure 2. Quality layer- Left: False colour composite of R2A L3, Right: Quality layer

4.1 Absolute validation

Absolute validation becomes challenging due to the absence of surface measurements with the necessary spatial and spectral resolution for a specific site (Badawi et al., 2019). Synchronous ground measurements from RCN and pseudo invariant sites in India are used for absolute validation. Currently, there are five sites involved in RCN, which are located in the United States (Rail Road Playa-RVU), France (La Crau-LCFR), Namibia (Gobabeb-GONA), and China (Batou&Batou sand-BSCN&BTCN). All RCN sites are soil/desert sand targets as shown in figure3. Near simultaneous ground measurements during R2A/RS2 overpasses at Thar Desert sand-Lanela, snow-Gulmarg, river sand-Mandarna, soils-Shadnagar and crops-Attabira are taken with field spectro-radiometer. Data sets over these sites since 2017 are considered for validation. Ground measurements are convolved (2) with sensor’s spectral response function and then compared.

$$\rho(\lambda)_i = \frac{\int_{\lambda 1}^{\lambda 2} \rho(\lambda) S_i(\lambda) d\lambda}{\int_{\lambda 1}^{\lambda 2} S_i(\lambda) d\lambda} \quad (2)$$

Where ρ(λ) is reflectance measured on ground and S(λ) is spectral response function of the sensor and ‘i’ is the band number. Depending on site homogeneity and number of samples collected from ground, corresponding mean values from SR products are taken and plotted for each $\rho(\lambda)_i$ for each band. RMSE and SSE are calculated using (3) and (4).The correlation coefficient for SR products of R2A and RS2 with ground measurements exceeds 0.9 for all bands except band 5, as detailed in Table 2. All absolute validation results are presented as scatter plots (X-axis: Ground measurements, Y-axis: SR of RS2/R2A) in Figures 4 and 5 for L3/AW and L4, respectively.

$$RMSE = \sqrt{\sum \frac{(\rho_{ref} - \rho_{sensor})^2}{N}} \quad (3)$$

$$SSE = \sum_{i=1}^{N} (\rho_{ref} - \rho_{sensor})^2 \quad (4)$$

Where ρ_{ref} is ground measured reflectance or contemporary SR values, $\rho_{sensor}$is sensors reflectance and N is the number of points/observations.

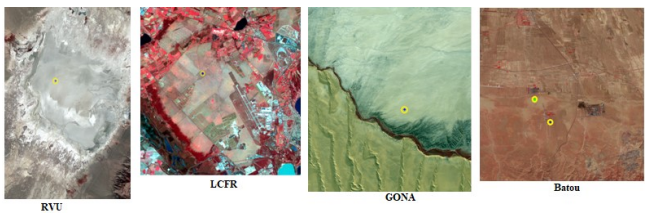

Figure 3. RCN sites as viewed by R2A L3 sensor, Site location -yellow circle

4.2 Relative validation

HLS products are utilized as reference data for relative validation purposes. The surface reflectance (SR) products of the L3 sensor are resampled to match the HLS spatial resolution of 30 meters, while the HLS products are resampled to the 56-meter resolution of the AW sensors. Additionally, the SR products from the L4 sensor are resampled to the 10-meter resolution of Sentinel-2.The spectral bands 3, 4, 5, and 6 of HLS are nearly equivalent to those of the L3/AW sensors, with the exception of a slight variation in the spectral resolution of band 4. Bands 2, 3, and 4 of the L4 sensor correspond to bands 3, 4, and 8 of Sentinel-2.

L4: Absolute Validation					
R2	**Slope**	**Offset**	**R^2**	**SSE**	**RMSE**
B2	0.886	0.000	0.965	0.019	0.025
B3	0.881	0.009	0.976	0.015	0.022
B4	0.747	0.043	0.898	0.040	0.037
RA					
B2	0.881	0.008	0.990	0.001	0.006
B3	0.901	0.010	0.990	0.002	0.011
B4	0.920	0.012	0.906	0.008	0.022
L3: Absolute Validation					
R2	**Slope**	**Offset**	**R^2**	**SSE**	**RMSE**
B2	0.701	0.007	0.951	0.011	0.016
B3	0.718	0.016	0.953	0.013	0.017
B4	0.648	0.060	0.934	0.015	0.018
B5	0.744	0.009	0.847	0.041	0.036
RA					
B2	1.016	-0.017	0.970	0.009	0.016
B3	0.974	0.010	0.963	0.011	0.018
B4	0.890	0.012	0.901	0.022	0.024
B5	0.928	-0.003	0.803	0.015	0.026
AW: Absolute Validation					
R2	**Slope**	**Offset**	**R^2**	**SSE**	**RMSE**
B2	0.979	-0.005	0.849	0.063	0.035
B3	1.012	-0.019	0.909	0.053	0.031
B4	0.826	0.060	0.806	0.024	0.022
B5	0.868	0.038	0.789	0.086	0.051
RA					
B2	0.878	0.027	0.989	0.003	0.014
B3	0.906	0.027	0.986	0.003	0.014
B4	0.848	0.052	0.925	0.012	0.027
B5	1.005	0.006	0.955	0.007	0.032

Table2. Absolute validation: RS2 & R2A SR-L4/L3/AW

The datasets considered for relative validation encompass a wide range of reflectance features, from low reflectance water bodies to high reflectance snow-covered areas, covering regions in India as well as CEOS sites such as Libya, Ivanpah Playa, Railroad Valley Playa, Sioux Falls, and Lake Tahoe.

R2A L3 and AW sensors show a good agreement of 95% and the RMSE is less than 0.02with HLS products as given in table3. RMSE of all sensors for all bands with respects to ground and contemporary measurements are given in figure 6. In case of RS2 sensors, the amount of agreement is around 80% for native radiometry and observed higher devotions in case of band5 as this band saturates for higher reflectance values. TOA products are also validated with level1C (L1C) products of Landsat-8 and Sentinel-2. The results of relative validation in the form of scatter plots for L4 SR and TOA are shown in figures7-10. False colour composite (FCC-Red: B4, Green: B3 & Blue: B2) TOA and SR products of L4 sensor are displayed in figure11. Relative validation of SR and TOA products of RS2/R2A AW and L3 sensors are given in figures 12-19.

The TOA values show greater deviations due to variations in illumination and atmospheric conditions at the time the images were captured. The average time difference between the contemporary images and the RS2/R2A images is approximately seven days. Since SR products are corrected for atmospheric effects and illumination geometry, the slope values are closer to 1.

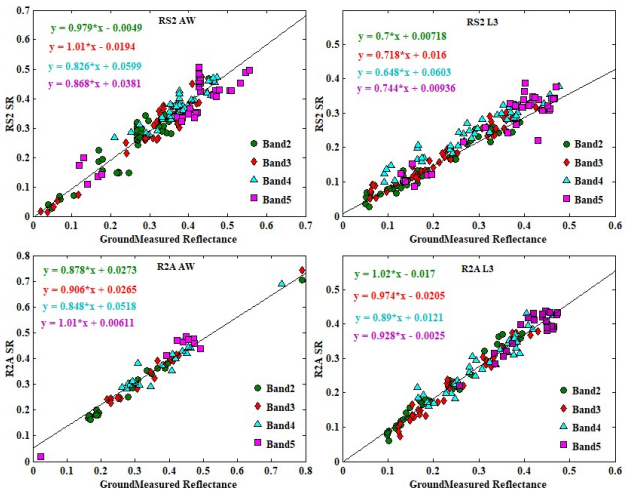

Figure 4. Absolute validation of RS2/R2A: L3/AW

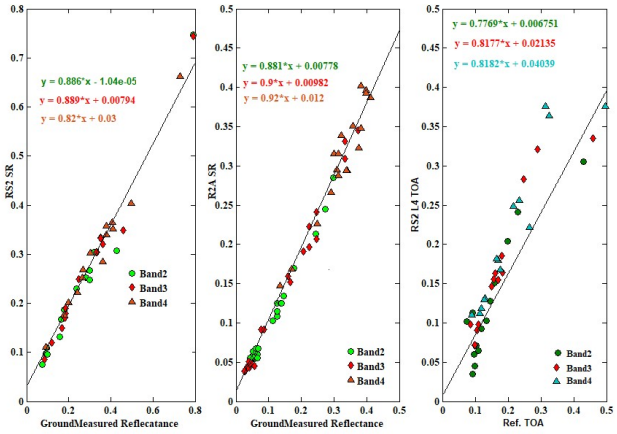

Figure 5. Absolute validation: Left: R2 L4-SR, Middle: R2A L4-SR, Right:RS2 L4-TOA versus ground simulated TOA

4.3 Intra sensor validation

Despite the similar spectral and spatial configurations of RS2 and R2A, differences in measured reflectances were observed. Combining both satellites reduces the temporal resolution. To address this, radiometric harmonization was performed on the SR products of RS2 sensors to allow comparison with R2A sensors.This process corrected the slight intra-sensor deviations present in the native radiometry. Relative validation was conducted before and after harmonization relative to R2A. The FCC of Figure 20 depicts the harmonized SR product of RS2 L3 along with R2A L3 image. Figures 21 and 22 present the cross-validation results, demonstrating improved slopes following harmonization.

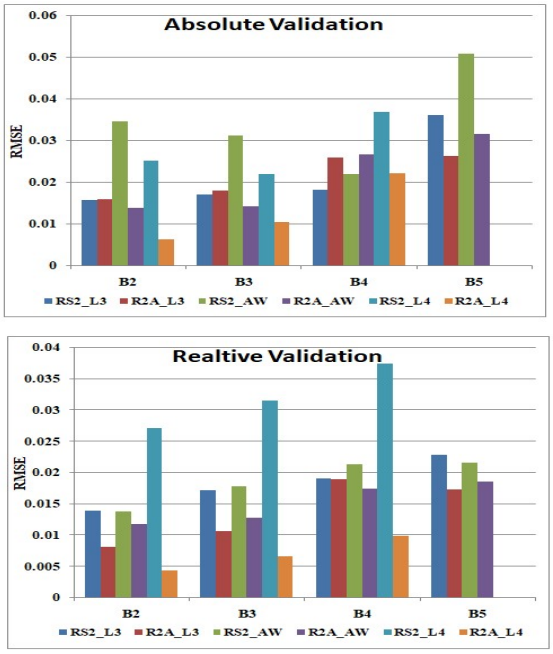

Figure 6. RMSE for absolute and relative validation of RS2/R2A

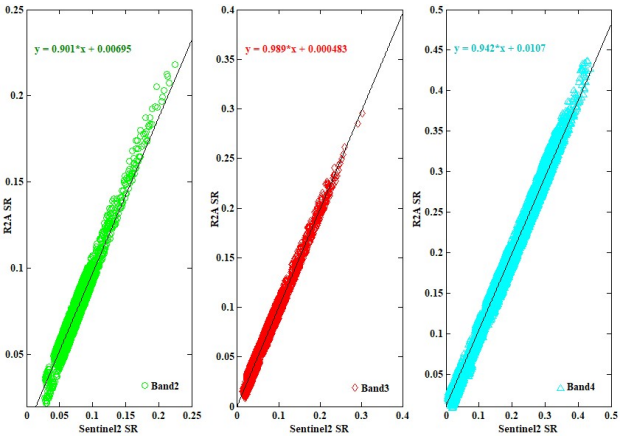

Figure 7. Relative validation: R2A L4-SR

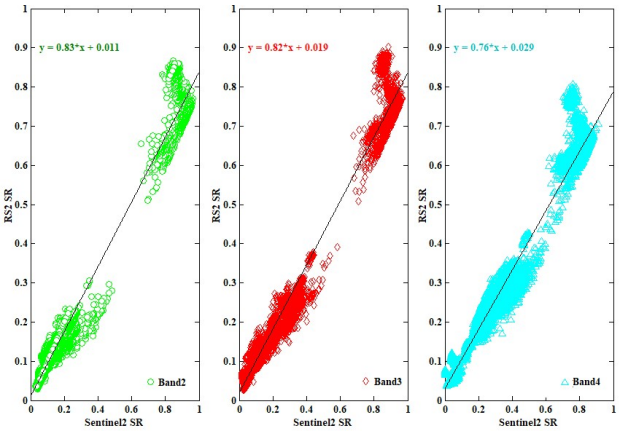

Figure8. Relative validation: R2 L4-SR

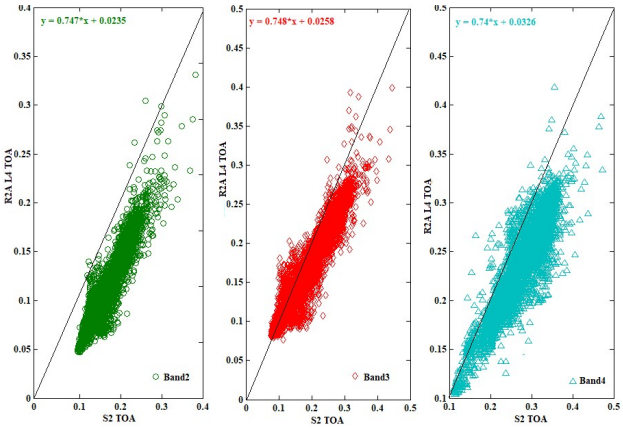

Figure 9. Relative validation: R2A L4-TOA

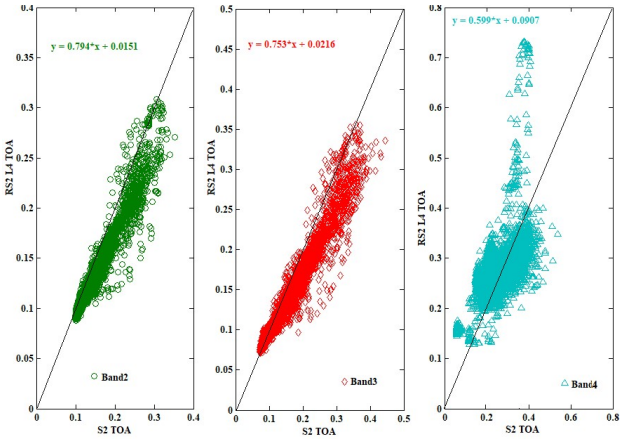

Figure 10.Relative validation: RS2 L4-TOA

Figure 11.R2A&RS2-L4, Left: TOA, Right: SR

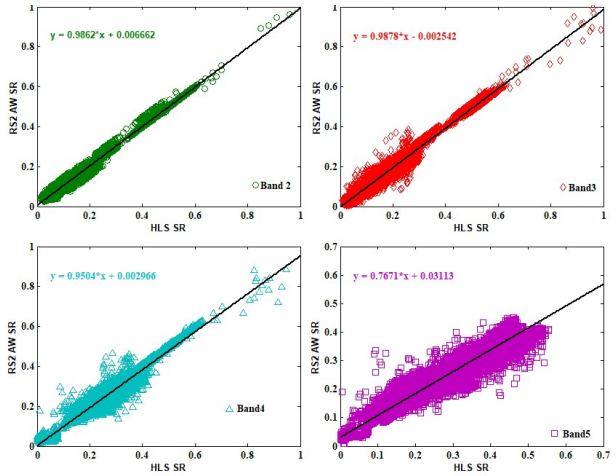

Figure 12.Relative validation: RS2 AW-SR

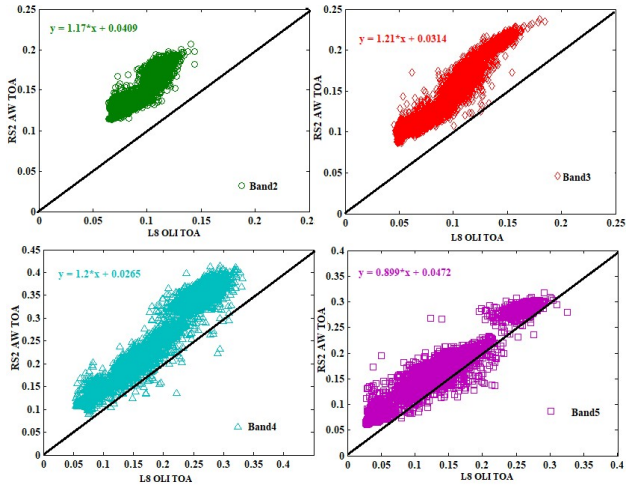

Figure 13.Relative validation: RS2 AW-TOA

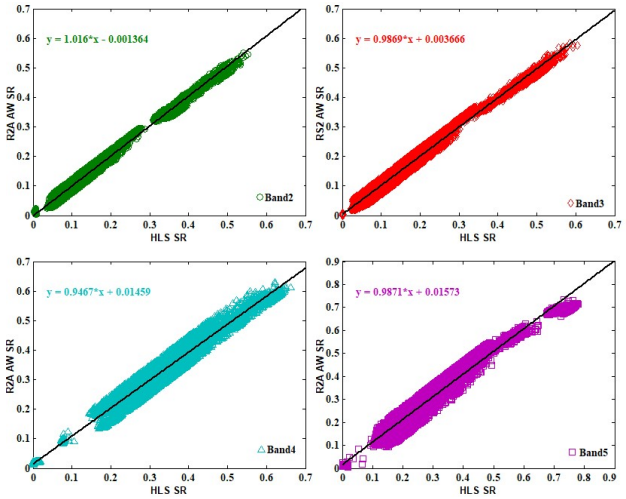

Figure 14.Relative validation: R2A AW-SR

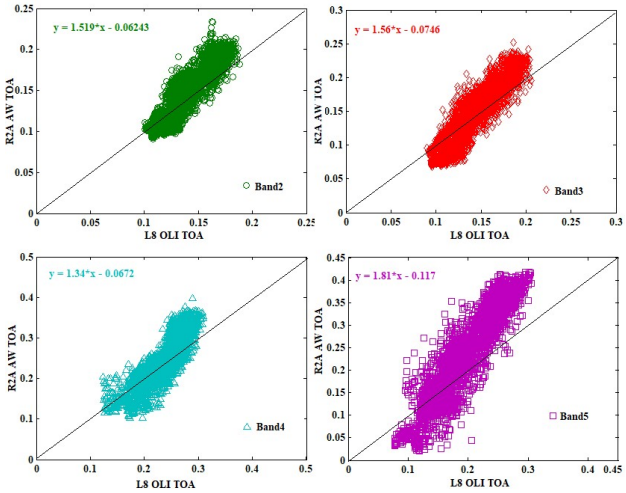

Figure 15.Relative validation: R2A AW-TOA

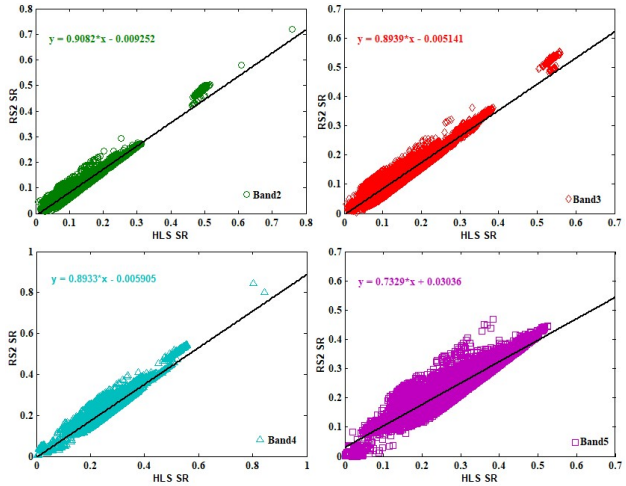

Figure 16.Relative validation: RS2 L3-SR

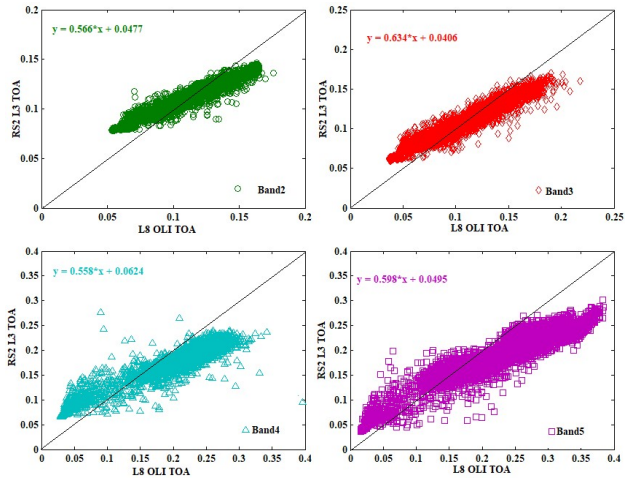

Figure 17.Relative validation: RS2 L3-TOA

L4: Relative Validation					
R2	**Slope**	**Offset**	**R^2**	**SSE**	**RMSE**
B2	0.827	0.011	0.982	7.349	0.027
B3	0.817	0.019	0.977	9.995	0.032
B4	0.758	0.029	0.964	14.010	0.037
RA					
B2	0.901	0.007	0.942	0.155	0.004
B3	0.989	0.000	0.968	0.361	0.007
B4	0.942	0.011	0.991	0.796	0.010
L3: Relative Validation					
R2	**Slope**	**Offset**	**R^2**	**SSE**	**RMSE**
B2	0.908	-0.009	0.956	5.892	0.014
B3	0.894	-0.005	0.959	8.954	0.017
B4	0.893	-0.006	0.938	10.940	0.019
B5	0.733	0.030	0.926	15.660	0.023
RA					
B2	1.009	-0.005	0.986	3.339	0.008
B3	1.009	-0.009	0.993	5.664	0.011
B4	1.004	-0.017	0.971	15.960	0.019
B5	0.982	-0.014	0.984	12.130	0.017
AW: Relative Validation					
R2	**Slope**	**Offset**	**R^2**	**SSE**	**RMSE**
B2	0.986	0.007	0.971	6.500	0.014
B3	0.988	-0.003	0.967	10.720	0.018
B4	0.950	0.003	0.967	14.830	0.021
B5	0.768	0.031	0.959	15.810	0.022
RA					
B2	1.016	-0.001	0.993	4.185	0.012
B3	0.987	0.004	0.994	4.946	0.013
B4	0.947	0.015	0.991	9.158	0.017
B5	0.987	0.016	0.984	24.510	0.019

Table3. Relative validation: RS2 & R2A SR-L4/L3/AW

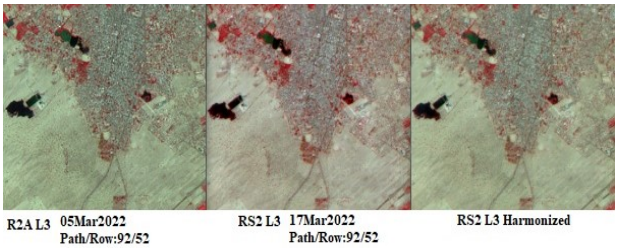

Figure 20.Left: RS2A L3, Middle: RS2 L3, Right: Harmonized RS2 L3

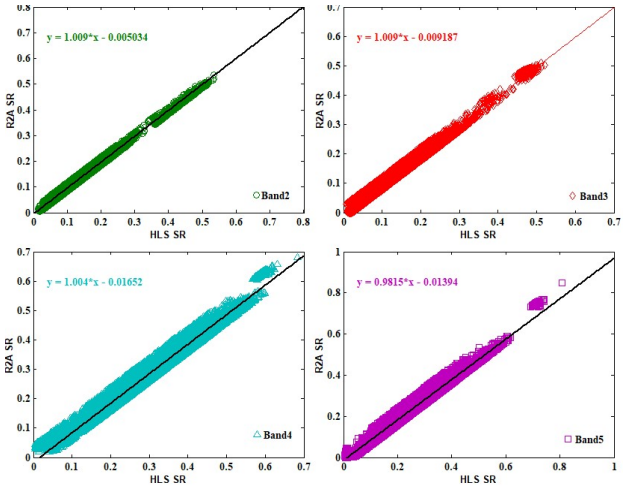

Figure 18. Relative validation: R2A L3-SR

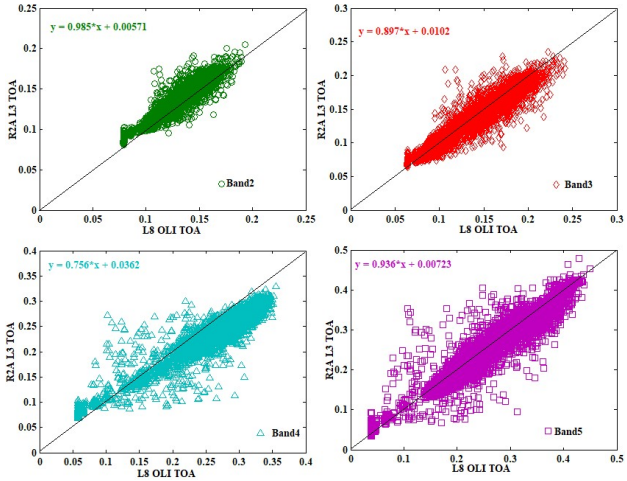

Figure 19.Relative validation: R2A L3-TOA

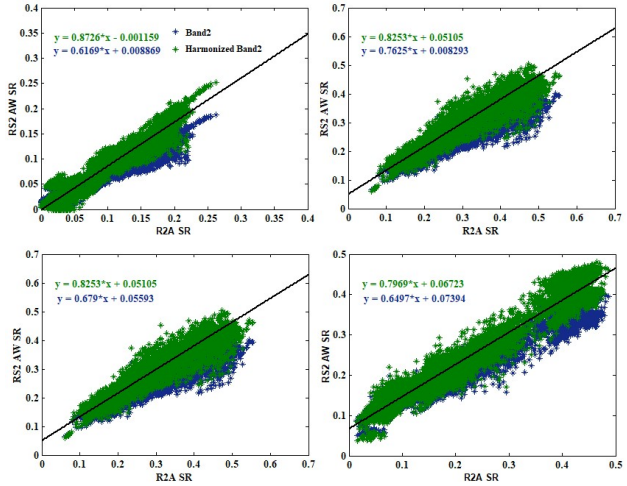

Figure 21.Intra sensor validation: Harmonized RS2 AW with R2A AW

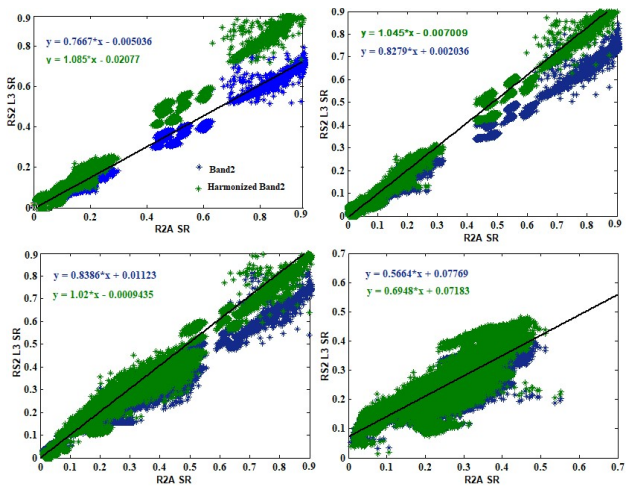

Figure 22.Intra sensor validation: Harmonized RS2 L3 with R2A L3

5. Conclusion

A frame work to generate ARD products from RS2/R2A sensors is developed to ensure the interoperability and increased temporal coverage. A thorough analysis was conducted to ensure the long-term accuracy and reliability of surface reflectance products from RS2/R2A sensors. The results demonstrate a high degree of accuracy and consistency of the satellite-derived surface reflectance products across different spectral bands when compared with in-situ measured surface reflectance and HLS products. The agreement for bands 2, 3 and 4 is better than 90% for R2A and better than 80% for RS2 with ground measured reflectances. A minor deviation in the surface reflectance values of the SWIR band (B5) of RS2, caused by saturation at higher reflectance, is nullified after radiometric harmonization with R2A. The minor and potential biases between the surface reflectance of HLS and RS2/R2A can be caused due to the atmospheric correction models and spectral band differences. This can be reduced after radiometric harmonization with spectral bandpass adjustment (SBAF). ARD data sets are thoroughly validated with both ground and satellite based products and can be utilized for time series analysis for various Earth resources.

Acknowledgement

The authors are sincerely thankful to the NRSC & ISRO teams who helped in direct and indirect ways to accomplish the generation of ARD data sets from RS2/R2A sensors. The authors are also thankful to RadCalNet team for the ground measurements.

References

Badawi M, Helder D, Leigh L, Jing X., 2019. *Methods for* earth-observing satellite surface reflectance validation. *Remote Sensing*, Vol.11,No.13, pp: 1543.

Bouvet M, Thome K, Berthelot B, Bialek A, Czapla-Myers J, Fox NP, Goryl P, Henry P, Ma L, Marcq S, Meygret, A., Wenny, B.N., Woolliams,E.R., 2019.RadCalNet: A radiometric calibration network for Earth observing imagers operating in the visible to shortwave infrared spectral range. *Remote Sensing*, Vol.11,No.20, pp: 2401.

Canty, M.J., Nielsen, A.A., 2007.Investigation of alternative iteration schemes for the IR-MAD algorithm.In*Proceedings of SPIE - The International Society for Optical Engineering.*

Chavez, P.S., 1996. Image-based atmospheric corrections-revisited and improved. *Photogrammetric engineering and remote sensing*, Vol. 62,No.9, pp: 1025-1035.

Garrigues, Sebastien, JulienChimot, Melanie Ades, Antje Inness, Johannes Flemming, Zak Kipling, Istvan Laszlo et al. 2022. Monitoring multiple satellite aerosol optical depth (AOD) products within the Copernicus Atmosphere Monitoring Service (CAMS) data assimilation system.*Atmospheric Chemistry and Physics,* Vol.22, No.22 pp: 14657-14692.

Lewis, A.; Lacey, J.; Mecklenburg, S.; Ross, J.; Siqueira, A.; Killough, B.; Szantoi, Z.; Tadono, T.; Rosenavist, A.;Goryl, P.; et al.2018.CEOS Analysis Ready Data for Land (CARD4L) Overview.*IGARSS 2018*, Valencia, Spain,pp: 7407–7410.

Nazeer, M., Ilori, C.O., Bilal, M., Nichol, J.E., Wu, W., Qiu, Z., Gayene, B.K., 2021. Evaluation of atmospheric correction methods for low to high resolutions satellite remote sensing data, *Atmospheric Research*, Vol.249, pp: 105308.

Ronneberger, O., Fischer, P., Brox, T., 2015. U-net: Convolutional networks for biomedical image segmentation. In *Medical image computing and computer-assisted intervention–MICCAI 2015: 18th international conference*, Munich, Germany, proceedings, part III 18,pp: 234-241.

Siqueira A, Lewis A, Thankappan M, Szantoi Z, Goryl P, Labahn S, Ross J, Hosford S, Mecklenburg S, Tadono T, Rosenqvist A.,2019. CEOS analysis ready data for land–an overview on the current and future work, In*IGARSS 2019-IEEE International Geoscience and Remote Sensing Symposium*, pp:5536-5537.

Vermote EF, Tanré D, Deuze JL, Herman M, Morcette JJ., 1997.Second simulation of the satellite signal in the solar spectrum, 6S: An overview. *IEEE transactions on geoscience and remote sensing*. Vol. 35, No.3, pp: 675-86.

Wulder, M.A.; Loveland, T.R.; Roy, D.P.; Crawford, C.J.; Masek, J.G.; Woodcock, C.E.; Allen, R.G.;Anderson, M.C.; Belward, A.S.; Cohen, W.B.; et al.2019.Current Status of Landsat Program, Science, andApplications.*Remote Sensing of Environment*,Vol. 225, pp: 127–147.